Power law scaling model predicts N_2O emissions along the Upper Mississippi River basin

Alessandra Marzadri[a], Daniele Tonina[b], Alberto Bellin[a]

[a]*Department of Civil, Environmental and Mechanical Engineering, University of Trento, Trento, 38123, Italy*

[b]*Center for Ecohydraulics Research, University of Idaho, Boise, ID 83702, USA*

Abstract

Nitrous oxide, N_2O, is widely recognized as one of the most important greenhouse gases, and responsible for stratospheric ozone destruction. A significant fraction of N_2O emissions to the atmosphere is from rivers. Reliable catchment-scale estimates of these emissions require both high-resolution field data and suitable models able to capture the main processes controlling nitrogen transformation within surface and subsurface riverine environments. Here, we test and validate a recently proposed parsimonious, yet effective, model to predict riverine N_2O fluxes along the main stem of the Upper Mississippi River (UMR). The model parameterizes N_2O emissions by means of two denitrification Damköhler numbers; one accounting for processes occurring within the hyporheic and benthic zones, and the other one within the water column, as a function of river size. Comparison of predicted N_2O gradients between water and air (ΔN_2O) with those quantified from field measurements validates the predictive performance of the model and allow extending previous findings to large river networks including highly regulated rivers with cascade reservoirs and locks. Results show the major role played by the water column processes in contributing to N_2O emissions in large rivers. Consequently, we infer that along the UMR, characterized by regulated flows and large channel size, N_2O production occurs chiefly within this surficial riverine compartment, where the suspended particles may create anoxic microsites, which favor denitrification.

Keywords: Nitrous oxide emissions, River network, Upper Mississippi River

1. Introduction

The use of synthetic fertilizers and fossil fuel combustion, led the atmospheric concentration of nitrous oxide (N_2O) to increase, reaching the today high levels [1]. Besides being an important greenhouse gas (GHG), N_2O is recognized as the dominant stratospheric ozone-depleting substance [2]. According to the Intergovernmental Panel of Climate Change (IPCC) [3] 4.5 million tonnes of N_2O per year [3] are produced by agriculture, with 25% consisting of indirect emissions originating from runoff and leaching of fertilizers. Excess of fertilizers used for food and energy production enters the stream network from run-off, groundwater flow or atmospheric deposition and here they undergo a number of transformations and ultimately part of the reactive nitrogen returns to the atmosphere as N_2O, chiefly through denitrification. In this paper, we focus on the contribution to N_2O emissions of the following three riverine environmental compartments: water column, benthic area and hyporheic zone [4, 5]; which together accounts for $\sim 10\%$ of the total N_2O emissions from lotic systems [6, 7, 8]. In these systems, N_2O emissions are attributable to different biogeochemical processes (i.e. nitrification, denitrification and reduction of nitrate to ammonia (DNRA)) [9] but still nitrification-denitrification represents the most important pathway that converts dissolved inorganic nitrogen (DIN) species (ammonium, NH_4^+, and nitrate, NO_3^-) to N_2O. Production of N_2O may be controlled by numerous geochemical (i.e., pH, temperature, DIN, dissolved oxygen: DO, and dissolved organic carbon: DOC) and hydrological (i.e. water discharge, river morphology and surface water conditions) factors [6, 10, 4, 11, 12, 13]. Although the main processes and the environmental factors controlling N_2O emissions have been the subject of recent studies, [see e.g. 14, and citations therein], few tools are available to estimate these emissions at the catchment and larger scales [14, 15, 5].

A major difficulty in modeling N_2O emissions at the catchment scale is the large spatial and temporal variability of reactive nitrogen input as well as of the parameters controlling its transformations [16, 17]. The lack of detailed continuous measurements of in-stream N_2O concentrations and the low spatial coverage of data, led to a major development of regression models that bind observed emissions with specific biogeochemical quantities such as nitrate [7, 18, 10, 19], dissolved oxygen [11], dissolved organic carbon [20] and temperature [21]. Looking at the river networks spatial scale, several studies showed that N_2O emissions decrease exponentially as a function of stream order [22]. This suggests that not only reactive nitrogen loads but also hydromorphology influence N_2O emissions. Recently, Marzadri et al. [5] proposed a parsimonious, in term of parameters, model that was able to interpret the data collected in both the LINXII experiment [23, 4] and a detailed survey in the Kalamazoo river basin [24, 18]. The model provides N_2O emissions, normalized with respect to the DIN mass flux, as a function of a suitable Damköhler number, defined as the ratio between a characteristic transport time and a characteristic reaction time [25], which quantifies the effect on emissions of the permanence of the reactive nitrogen in an environment favourable to reaction. The model identified two end-member expressions, under the form of scaling laws: an upper bound (UB) scaling law to be applied when emissions are controlled by hyporheic and benthic processes and a lower bound (LB) scaling law when benthic processes dominate and hyporheic processes are weak. The analysis of 400 reaches around the world, suggested the introduction of a third scaling law, coined as stream water column (WC) scaling law, which accounts for processes occurring chiefly within the water column. The use of the WC equation is recommended in large and deep rivers where the hyporheic zone has negligible effects on N_2O emissions [5]. In this formulation, the proposed 3-equation model accounts for the decline in the relative contribution of the hyporheic zone to N_2O emissions with respect to benthos and water column, as stream size increases. It is also fully characterized with measured or derived quantities and does not require any calibration or fitting to data. This is a key condition for its use as a predictive model.

The UB and LB scaling laws were verified on an independent data set of 400 stream and river reaches (not used to develop the models) in three continents, obtaining good performances [5]. However, the WC scaling laws was derived from that 400-reaches data set because no large and deep rivers were contained in the original set of data used to derive UB and LB (i.e. the LINXII and Kalamazoo river data). Consequently, the WC scaling law was not validated. Additionally, Marzadri et al. [5] did not identify nor suggested the conditions under which LB performs better than WC scaling law and whether their performance is stream size dependent. Moreover, both LB and WC scaling laws depend on denitrification uptake rate [23, 26], whose effects on model performance has not been previously addressed.

Here, we addressed these issues and we also tested our hypothesis that there is a river size threshold beyond which the WC equation is a better predictor of N_2O emissions than LB because the importance of the benthic processes reduces as the stream size increases. We addressed our goal by comparing LB and WC models' predicted N_2O emissions against an independent set of high-spatial resolution field measurements recently collected by Turner et al. [13] along the Upper Mississippi River (hereafter UMR). The UMR is a large system (widths larger than 80 m) with increasing size and discharge suitable for the validation of the WC scaling law.

2. Materials and Methods

UMR drains one of the most intensive agricultural areas of the world. The study reach is the 350 km long portion of the UMR between the Lower St. Anthony Falls (MN) Lock and Dam to the Lock and Dam 8 near Genoa (WI) for a total of 64,770 mi^2 contributing area. Streambed material is mainly composed by sand and finer sediments [27, 28], with median grain size, $d_{50} \cong 0.7$ mm [27]. There are 13 gauging stations along the study site with 3 major tributaries: the Minnesota, St. Croix and Chippewa. Flows is regulated by several dams and locks that form backwaters. Data were collected by Turner et al. [13] between 1^{st} and 3^{rd} of August 2015 when mean daily discharges varied spatially between 145 and 936 m^3/s and channel widths between 80 and 3,200 m.

2.1. Input data

2.1.1. Water quality data

We used a data set composed by 1,553 GPS geo-referenced (uniquely identifiable by latitude and longitude) field measurements of in-stream dissolved N_2O concentration ($[N_2O]$, $mgN_2O - N/L$) [13], the saturation percentage of nitrous oxide ($N_2O_{sat}\%$)[13] and the in-stream nitrate concentration, $[NO_3^-]$ (mgN/L) [29]. Data were collected with a boat-mounted flow-through sampling system [30] with a 200 m average spatial resolution (minimum distance $\sim$ 7cm and maximum distance $\sim$ 1km) along the study reach (see Figure 1). Measurements were performed at daylight [30, 13, 29] with the overall objective to obtain *"a regional-scale assessment of* N_2O *concentration patterns in the UMR"* [13]. Consequently, even if all the collected data represented conditions at a given time, their spatial coverage supported well our goal to test the upscaling capability of the Marzadri et al.'s model [5], namely to predict N_2O emissions at the large regional scale. After removing 358 measurements taken from lateral (i.e., outside the river's main stem) natural lakes or reservoirs and averaging 279 replicates the final usable dataset was composed by 916 independent measurements.

The work by Turner et al. [13] reported only the mean water temperature for the entire UMR ($T = 23.8^oC$ with a standard deviation of $0.6\,^oC$) during the surveying period (August 1-3, 2015). To spatially distribute the water temperature along the UMR, we assigned to the reaches, identified according to their Hydrological Unic Code (HUC-8) shown in Figure 1 and Table 1, the median temperature reported by Loken et al. [29] for the same sampling period. The mean of the assigned temperatures ($T = 23.6^oC$ and 0.6 standard deviation) compared well with the mean value of 23.8^oC reported by Turner et al. [13].

Similarly, the in-stream NH_4 concentrations (mgN/L) along the UMR were spatially distributed proportionally to the spatial distribution of ammonium plus ammonia values, NH_4, reported in Loken et al. [29].

HUC8	**Name**	**Range of measurements**	**Median** NH_4 (mgN/L)	**Median** T (°C)
07010206	Twin - Cities	1 - 367	0.036	23.01
07040001	Rush - Vermillion	369 - 911	0.012	24.06
07040003	Buffalo - Whitewater	912 - 1429	0.020	24.38
07040006	La Crosse - Pine	1430 - 1500	0.008	23.4
07060001	Coon - Yellow	1500 -1522	0.014	24.0

Table 1: Median values of ammonium plus ammonia (NH_4) and water temperature (T) variation along the main stem of the Upper Mississippi River.

2.1.2. Stream hydraulics data

Discharge values, Q, were quantified as the average of the daily values measured between August 1^{st} and 3^{rd}, 2015 at the 13 gauging stations operated by the U. S. Geological Survey, USGS, and the U. S. Army Corps of Engineers stations, USACE, [31] (see Figure 1 and Table 2) along the study site. Their measurements accounted for the in-flows of the major tributaries and showed sudden increases in discharge at their confluences. Overall measured water discharge increases almost linearly with distance (see Figure A.1 in the Appendix), with major confluences, thereby allowing the use of linear interpolation to compute Q in the reaches between them. This is consistent with the hypothesis of a contribution proportional to the upstream drainage area, as showed in Figure A.1 of the Appendix.

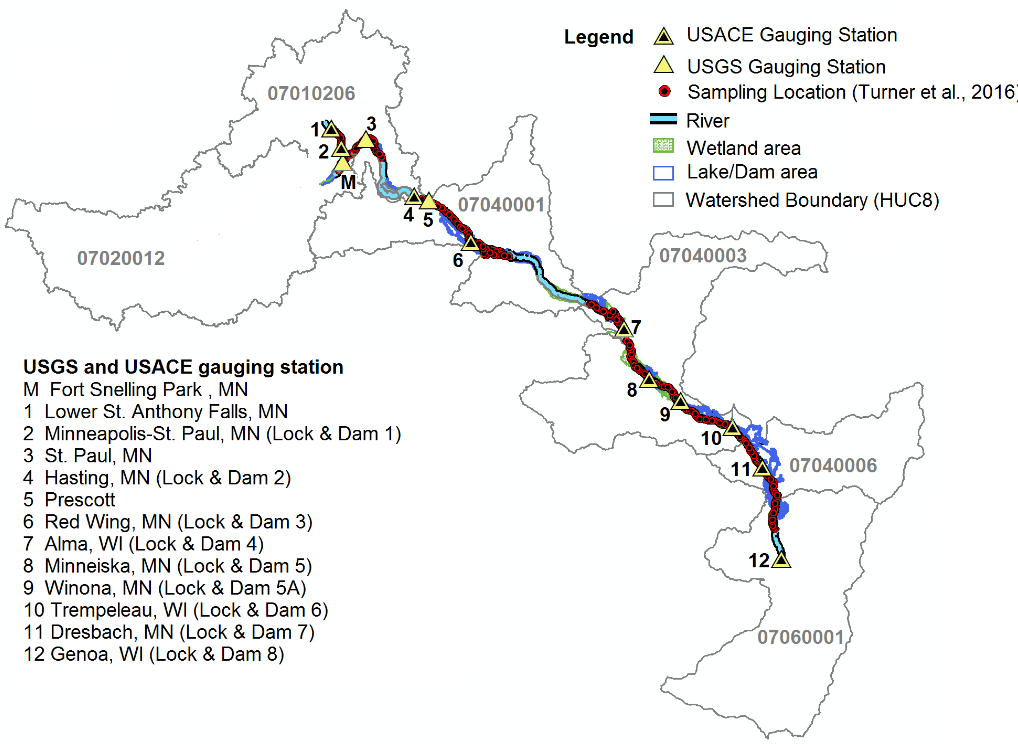

Figure 1: Map of the analyzed part of the Upper Mississippi River (UMR) for which data of water-air nitrous oxide gradient (ΔN_2O) are provided by Turner et al. [13] (red points).

Agency	**River**	**Station name**	**Lat.**	**Long.**	**Q**$^{(a)}$
(-)	(-)	(-)	(dec. Deg)	(dec. Deg)	(m^3/s)
USGS	MNR	Fort Snelling Park , MN	44.87028	-93.1922	145.470
USACE	UMR	Lower St. Anthony Falls, MN	44.97833	-93.2469	198.901
USACE	UMR	Lock and Dam 1, MN	44.91528	-93.2006	331.344
USGS	UMR	St. Paul, MN	44.94444	-93.0881	352.112
USACE	UMR	Hasting, MN (Lock and Dam 2)	44.75972	-92.8686	352.112
USGS	UMR	Prescott, MN	44.74583	-92.8000	530.528
USACE	UMR	Red Wing, MN (Lock and Dam 3)	44.6100	-92.6103	494.656
USACE	UMR	Alma, WI (Lock and Dam 4)	44.32556	-91.9203	722.160
USACE	UMR	Minneska, MN (Lock and Dam 5)	44.16111	-91.8108	814.672
USACE	UMR	Winona, MN (Lock and Dam 5A)	44.08833	-91.6689	824.112
USACE	UMR	Trempeleau, WI (Lock and Dam 6)	43.99972	-91.4383	878.864
USACE	UMR	Dresbach, MN (Lock and Dam 7)	43.86694	-91.3072	838.272
USACE	UMR	Genoa, WI (Lock and Dam 8)	43.5700	-91.2317	936.448

$^{(a)}$ Q is the average daily discharge at the gauging station between 1-3 August 2015.

Table 2: Characteristics of the twelve gauging stations along the Upper Mississippi River (UMR) and the gauging station along the Minnesota River (MNR).

Reach scale estimates of hydraulic depth, D (m), were obtained as a function of Q, expressed in m^3/s, through the power law scaling proposed by Miller et al. [32]:

$$\mathrm{D} = 0.18\,\mathrm{Q}^{0.47}\,(\mathrm{r}^2 = 0.73) \tag{1}$$

and those of channel width, W (m), were obtained from Google Earth Pro (Google Earth Pro, 2017) at each sampling site location.
Reach-scale flow velocities, V (m/s), were obtained as the ratio between Q and the cross sectional channel area ($W \cdot D$) under the hypothesis of wide rectangular channel:

$$\mathrm{V} = \frac{\mathrm{Q}}{\mathrm{W} \cdot \mathrm{D}} \tag{2}$$

The stream slope s_0 (-) was quantified by means of the Manning's formula [33]:

$$\mathrm{s}_0 = \left(\frac{\mathrm{Mn} \cdot \mathrm{V}}{\mathrm{D}^{2/3}}\right)^2 \tag{3}$$

by assuming prevailing uniform flow conditions in a wide channel, such that the hydraulic water depth D can be used in lieu of the hydraulic radius. The Manning's coefficient $Mn = 0.026$ ($s/m^{1/3}$) was inherited from previous hydraulic analysis of this system [34].

The resulting gentle stream slope, $s_0 < 0.02\%$ and fine streambed material are conducive to bed forms primarily composed by dunes [35], whose mean length (L) and height (H_d) were quantified with the formulation proposed by Yalin [36]: $L = 6D$ and $H_d = 0.167D$, respectively. The head variation at the water-sediment interface (h_m) is the main mechanism that drives stream water in and out of the streambed sediment through the hyporheic zone along the dune. It was quantified according to the formulation proposed by Shen et al. [37]:

$$\mathrm{h_m} = \frac{0.28 \cdot \mathrm{V}^2}{2\mathrm{g}}\left(\frac{\mathrm{H_d}}{0.34\mathrm{D}}\right)^{3/8} \tag{4}$$

where g is the gravitational acceleration (m/s^2).

Finally, we estimated the streambed hydraulic conductivity, K_h (m/s), according to the following expression proposed by Gomez-Velez et al. [38]:

$$\mathrm{K_h} = 119.06\,\mathrm{d}_{50}^{1.62} \tag{5}$$

which leaded to $\mathrm{K_h} = 9.2 \times 10^{-4}\,\mathrm{m/s}$ (in agreement with typical values of fine-medium sand [39]) and was assumed homogeneous and isotropic [40].

2.2. N_2O emission model

According to Marzadri et al. [5], we quantified the N_2O flux, FN_2O, as the product between its dimensionless expression, F^*N_2O, and the in-stream total flux of ammonium ($[\mathrm{NH}_4^+]$) and nitrate ($[\mathrm{NO}_3^-]$) (the two major species of dissolved inorganic nitrogen, DIN, responsible of N_2O production [41]): $FDIN_0 = V([\mathrm{NH}_4^+] + [\mathrm{NO}_3^-])$. The dimensionless flux F^*N_2O assumes the following expressions

$$\begin{cases} \mathrm{F^*N_2O_{,UB}} = 1.55 \times 10^{-7}(\mathrm{Da_{DHZ}})^{0.43},\, W \leq 10m \\ \mathrm{F^*N_2O_{,LB}} = 1.91 \times 10^{-8}(\mathrm{Da_{DHZ}})^{0.58},\, W > 30m \\ \mathrm{F^*N_2O_{,WC}} = 4.56 \times 10^{-6}(\mathrm{Da_{DS}})^{0.72},\, W > 30m \end{cases} \tag{6}$$

depending on the stream size. In equation (6), Da_{DHZ} and Da_{DS} are the two denitrification Damköhler numbers identified by Marzadri et al. [5] and whose importance depends on the size of riverine system, which was classified as small (width, $W \leq 10m$) and intermediate ($10 < W \leq 30$ m) streams and rivers ($W > 30m$) [42, 43]. Da_{DHZ} was defined as:

$$\mathrm{Da_{DHZ}} = \frac{\tau_{50}}{\tau_{\mathrm{D}}} = 17.810\,\mathrm{g}\,\frac{\mathrm{D\,v_{fden}}}{\mathrm{K_h V^2}} \tag{7}$$

where τ_{50} is the median hyporheic residence time evaluated according to the formulation proposed by Elliott and Brooks [44] (see major details in Marzadri et al. [5]), τ_D is the time of denitrification ($\tau_D = D/v_{fden}$) with v_{fden} beings the uptake rate of denitrification[41]. This equation assumed dune topography with Yalin [36] scaling and Shen et al. [37] formulation for head variation at the water sediment interface.

In WC model, τ_{50} is replaced with the characteristic time of turbulent vertical mixing [45]:

$$\mathrm{t_m} = \frac{\mathrm{D}}{0.067\sqrt{\mathrm{g\,D\,s_0}}}, \tag{8}$$

thereby Da_{DS} assumes the following form [5]:

$$\mathrm{Da_{DS}} = \frac{\mathrm{t_m}}{\tau_\mathrm{D}} = 14.925\frac{\mathrm{v_{fden}}}{\sqrt{\mathrm{g\,D\,s_0}}} \tag{9}$$

2.2.1. Uptake rate of denitrification

The uptake rate of denitrification, v_{fden}, was evaluated according to two formulations, one proposed by Mulholland et al. [23] and the other one by Böhlke et al. [26].

Böhlke et al. [26] defined v_{fden} as the ratio between the areal uptake rate of denitrification, U_{den}, and the mean flow depth ($v_{fden} = U_{den}/D$) and proposed four different models to estimate U_{den} as a power law function of in-stream NO_3 concentrations. Here, we adopted the model that they obtained by combining and weighting the data from the LINXII [23] and UMR datasets in order to reflect the relative contributions of the different environments characterizing the two datasets and to attribute some preference for $^{15}N_2$ data.

The formulation of Mulholland et al. [23] is:

$$log(v_{fden,M}) = -0.493log[\mathrm{NO_3}] - 2.975 \tag{10}$$

with $v_{fden,M}$ expressed in cm/s and $[NO_3]$ in μgN/L, whereas that of Böhlke et al. [26] is:

$$v_{fden,B} = \frac{17\,[\mathrm{NO_3}]^{0.51}}{D} \tag{11}$$

with $v_{fden,B}$ expressed in m/s and $[NO_3]$ expressed as μmolN/L.

2.3. Comparison between simulated and predicted values

The performance of the LB and WC models against measurements was assessed by comparing the water-air nitrous oxide gradient, ΔN_2O, provided by the model of Marzadri et al. [5] (equation (13)) against the estimate obtained from the field data provided by Turner et al. [13]:

$$\Delta N_2O = [N_2O] - [N_2O]_{eq} = [N_2O] - 100\frac{[N_2O]}{\%N_2O_{sat}}, \tag{12}$$

where $[N_2O]$ and $\%N_2O_{sat}$ were measured, and:

$$\Delta N_2O = \frac{FN_2O}{10^{-3}\,k_{N2O}} \tag{13}$$

where k_{N2O} (m/h) is the water-air piston velocity for N_2O and FN_2O is the estimated nitrous oxide emissions per unit area ($\mu gN_2O - N/m^2/h$). The former is represented as [46, 47, 48]:

$$k_{N2O} = k_{600} \left(\frac{Sc_{N2O}}{600} \right)^{-nw} \tag{14}$$

where nw is a dimensionless exponent, whose value depends on the state of the surface water [46], and Sc_{N2O} is the Schmidt number [$-$] evaluated as a function of the water temperature T (°C) by the following expression [47]:

$$Sc_{N2O} = 2056 - 137.11\,T + 4.317\,T^2 - 0.054\,T^3 \tag{15}$$

Here, we assumed $nw = 1/2$ because the UMR large width and discharge favours the development of waves at the air-water interface [46]. The gas transfer velocity, k_{600}, at a Schmidt number of 600 was evaluated by means of model 5 of Raymond et al. [48]:

$$k_{600} = 2841\,(V \cdot s_0) + 2.02 \tag{16}$$

where V and s_0 are estimated according to equation (2) and (3), respectively.

We evaluated the model's performance by using several metrics: the absolute error (AE_i), defined as:

$$\mathrm{AE_i} = |\Delta \mathrm{N_2O_i^{obs}} - \Delta \mathrm{N_2O_i^{sim}}|, \tag{17}$$

its average value $\overline{AE}$:

$$\overline{\mathrm{AE}} = \frac{1}{\mathrm{N}} \sum_{\mathrm{i=1}}^{\mathrm{N}} \mathrm{AE_i}, \tag{18}$$

the Nash Sutcliffe Efficiency index (NSE) [49] :

$$\mathrm{NSE} = 1 - \frac{\sum_{\mathrm{i=1}}^{\mathrm{N}} (\Delta \mathrm{N_2O_i^{obs}} - \Delta \mathrm{N_2O_i^{sim}})^2}{\sum_{\mathrm{i=1}}^{\mathrm{N}} (\Delta \mathrm{N_2O_i^{obs}} - \overline{\Delta \mathrm{N_2O_i^{obs}}})^2}, \tag{19}$$

the root mean square error ($RMSE$):

$$\mathrm{RMSE} = \sqrt{\frac{1}{N} \sum_{\mathrm{i=1}}^{\mathrm{N}} (\Delta \mathrm{N_2O_i^{obs}} - \Delta \mathrm{N_2O_i^{sim}})^2}, \tag{20}$$

the percentage of bias ($PBIAS$)

$$\mathrm{PBIAS} = \frac{\sum_{\mathrm{i=1}}^{\mathrm{N}} (\Delta \mathrm{N_2O_i^{obs}} - \Delta \mathrm{N_2O_i^{sim}})}{\sum_{\mathrm{i=1}}^{\mathrm{N}} (\Delta \mathrm{N_2O_i^{obs}})} \cdot 100 \tag{21}$$

and the ratio of $RMSE$ to the standard deviation (SD) of the measured data (RSR):

$$\mathrm{RSR} = \sqrt{\frac{\sum_{\mathrm{i=1}}^{\mathrm{N}} (\Delta \mathrm{N_2O_i^{obs}} - \Delta \mathrm{N_2O_i^{sim}})}{\sum_{\mathrm{i=1}}^{\mathrm{N}} (\Delta \mathrm{N_2O_i^{obs}} - \overline{\Delta \mathrm{N_2O^{obs}}})}} \tag{22}$$

where N is the number of data (i.e. $N = 916$), and the superscripts ^{obs} and ^{sim} represent measured and simulated values of ΔN_2O, respectively. Furthermore, $\overline{\Delta N_2 O^{obs}}$ is the mean of the observations.

Interpretation of these indexes to quantify whether a model is satisfactory or not were based on the guidelines suggested by Moriasi et al. [50], who proposed that model simulations are satisfactory when $NSE > 0.50$, $RSR < 0.70$, and $PBIAS < \pm 25\%$.

3. Results and Discussion

All performance indexes indicated that the WC scaling law performed better than the LB and UB scaling laws for large rivers (Table 3). Only the WC model met all targets for the metrics used to assess the errors [50] (Table 3). Visual inspection of Figure 2, which shows predicted vs measured ΔN_2O, also confirms the better performance of WC scaling law compared to the other two scaling laws (with the 1:1 line passing through the data) and the poor performance of both UB and LB models. These results were supported by the analysis of correlation between AE_i and $\Delta \mathrm{N_2O_i^{obs}}$ shown in Figure A.2. AE_i obtained with the WC and LB scaling laws were uncorrelated with the measured ΔN_2O. Therefore, the total error may reduce significantly when the emissions are aggregated (i.e. integrated) over the relevant (sub)catchments or higher scales.

As expected, the UB scaling law strongly overestimated ΔN_2O (Figure 2a), because it was developed for small streams, where N_2O emissions chiefly originate from the hyporheic zone, while measurements analyzed here were taken in a large river. This result confirmed the observation of Marzadri et al. [5], who argued that hyporheic zone was a negligible source of N_2O in rivers. The LB scaling law, which was applied for large rivers in the original

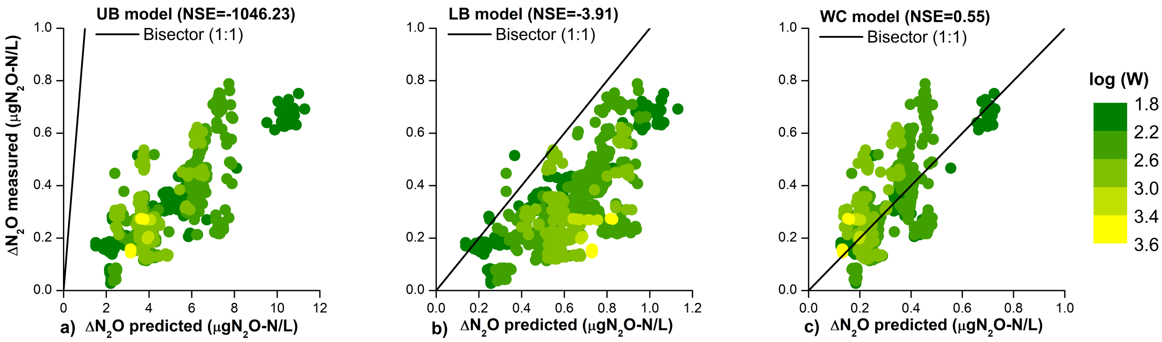

Figure 2: Comparison between predicted and measured water-air nitrous oxide gradient (ΔN_2O) along the Upper Mississippi River (UMR) by using: (a) the Upper Bound, UB, power law scaling; (b) the Lower Bound, LB, power law scaling and (c) the Water Column, WC, power law scaling (as in Marzadri et al. [5]). Color of the symbols shift from green to yellow as the width of the channel increases. The uptake rate of denitrification ($v_{f,denB}$) is estimated by using the equation (11)[26].

work of Marzadri et al. [5], overestimated ΔN_2O and had poor performance for the UMR data. This suggests that also the role of the benthic zone as a source of N_2O was negligible along the UMR (Figure 2b). Conversely the high performance indexes for the WC scaling law combined with the lack of correlation between AE_i and $\Delta N_2O_i^{obs}$ (notice the very small value of r^2 in Figure A.2c), suggests that processes within the water column were the main source of N_2O emissions.

In large riverine systems, such as UMR, we relate the major role played by the water column in controlling N_2O emissions to the presence of anoxic

Statistics	**UB model**	**LB model**	**WC model**
RMSE	5.019	0.344	0.104
SD	0.155	0.155	0.155
NSE	-1046.235	-3.912	0.547
PBIAS (%)	-1583.319	-107.512	-4.881
RSR	32.361	2.216	0.673

Table 3: Main statistical parameters: Root Mean Square Error (RMSE), Standard Deviation of observations (SD), Nash Sutcliffe Efficiency Index (NSE), Percentage of bias (PBIAS) and the ratio of the root mean square error to the standard deviation of measured data (RSR) for the three expressions (equation (6)) for small (UB) and large (LB and WC) rivers.

micro-sites associated to the suspended particle load that favor the microbially mediated process of denitrification along the surface water column rather than in the hyporheic and benthic zones [51, 52, 53]. Suspended sediments provide the supporting matrix of microbial colonies and biofilms and their density increase with discharge as reported in literature, since the pioneering work of Leopold and Maddock [54]. Empirical observations showed that suspended sediment concentration (SSC) depends on Q through the following power law expression: $\mathrm{SSC} = \mathrm{a}\,\mathrm{Q}^{\mathrm{b}}$ (with a and b obtained by regression with the specific experimental data) [55, 56]. We suggest that the negligible role of the hyporheic zone in large rivers was due to low hyporheic exchange, which in turn was due to low hydraulic conductivity of the streambed and low reaction rate constants as reported in the recent work by Reeder et al. [57]. This latter effect is due to the positive feedback between reaction and hyporheic exchange rate; higher downwelling velocities correlate with higher reaction rate constants [57], and the associate delivery of substrate biogeochemical components (i.e. NO_3) [58].

Figure 3 shows NSE as a function of the average channel width (14 bins of 61 data points and one bin with 62 points as described in the caption of table A.2 of the Appendix) with the modeled data obtained with LB and WC scaling laws (6) and with v_{fden} proposed by Mulholland et al. [23] (3a) and by Böhlke et al. [26] (3b). All performance indexes were reported for completeness in Tables A.2 and A.3 of the Appendix. The LB scaling law (red circle) with $v_{fden,M}$ showed better performance values than the WC scaling law for $W <\sim 175$ m, although both scaling laws had satisfactory performance (Figure 3a and Table A.2). However, as W increased NSE values of the LB scaling law decreased sharply becoming negative for $W >$ 286 m and with values of $PBIAS$ larger than 40% (see Appendix Table A.2 where the negative sign indicate that the model tends to overestimate the observations). For the WC scaling law, NSE gently decreases with W to almost a constant value of 0.36 after W nearly equal 400 m. All other indexes showed similar trends.

For LB and WC scaling laws with $v_{fden} = v_{fden,B}$, the LB scaling law had always negative NSE values and $PBIAS$ larger than 50%, regardless of reach size (Figure 3b and Table A.3). Conversely, with the WC scaling law NSE were almost constant and equal to 0.59 for $W > 230$ m and increased steeply with W smaller than 300 m, peaking to value of 0.93 for $W \cong 100$ m. Accordingly, the $PBIAS$ values were always negative and $< 15\%$ in absolute terms (Table A.3).

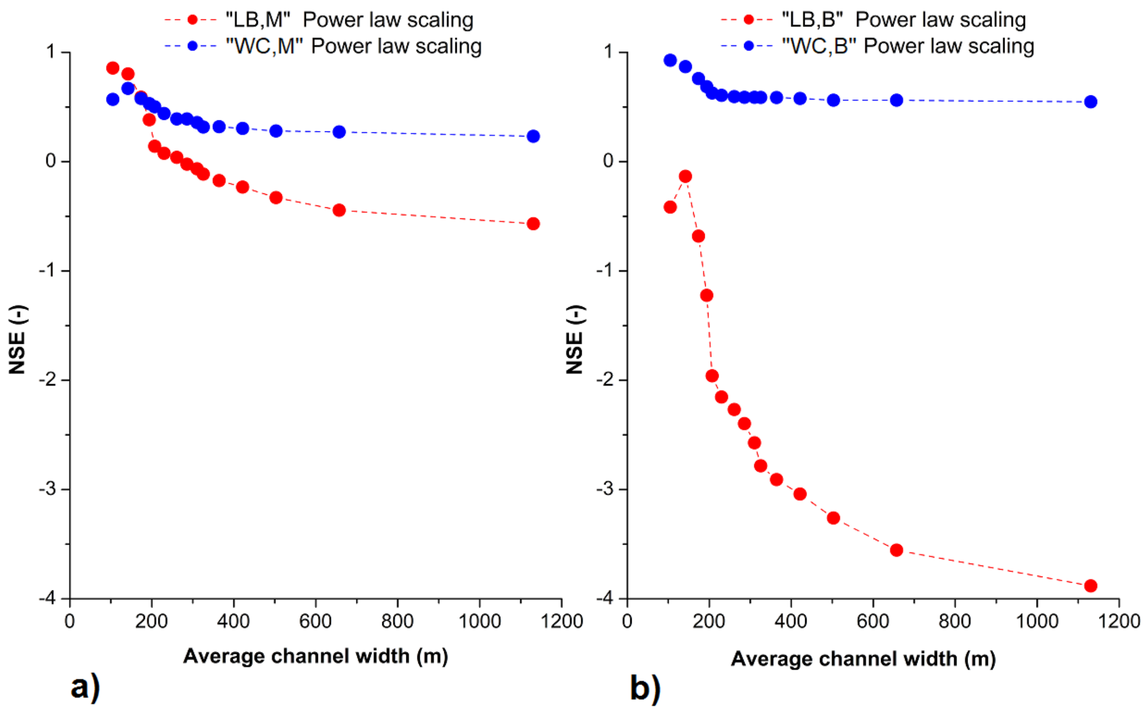

Figure 3: Goodness of prediction (Nash Sutcliffe Efficiency, NSE) of the Lower Bound, (LB red symbols), and the Water Column (WC blue symbols) power law models as a function of the average channel width. In panel (a) the uptake rate of denitrification, $v_{fden,M}$, is estimated using the relation proposed by Mulholland et al. [23]; while in panel (b) $v_{fden,B}$ is estimated using the relation proposed by Böhlke et al. [26]. Data are grouped in fifteen bins (14 with 61 points and the last one with 62 points).

These results are in agreement with previous studies [59, 60, 61, 62, 63] underlying how nutrient removal processes and consequently N_2O production scale across a broad range of stream sizes. According to Wollheim et al. [64] v_{fden} is a biological measure well suited for comparing biological activity in streams of different sizes and here, we showed the importance of this parameter to accurately predict N_2O emissions. The local physical and biogeochemical conditions that control the characteristic time of reaction (accounted here by using two different formulations for v_{fden}) influence the riverine environment that mainly controls N_2O emissions. For $W <\sim 175$ m similar results are obtained either by using LB and $v_{fden} = v_{fden,M}$ or WC and $v_{fden} = v_{fden,B}$ (see Figures 3a and 3b, respectively). Therefore, we suggest that accurate local measurements of this parameter are important to model ΔN_2O emissions accurately. It also underlines the strength of the proposed power law model to capture correctly these emissions as the boundary conditions change (i.e., the NO_3 load).

To emphasize this aspect, Figures 4a and 4b show the bin averaged values (bars represents $\pm$ 1 standard deviation) of ΔN_2O measured and predicted with LB and WC scaling laws, respectively with $v_{fden,M}$, and $v_{fden,B}$ (results of Figure 4 are supplemented by Appendix Tables A.2 and A.3).

The performance of the LB scaling law decreased with increasing river size regardless the model of v_{fden}, and it was lower than that of WC scaling law (Figure 4). Using $v_{fden,M}$, the LB scaling law predicted the measured emissions better than the WC scaling law for W <175 m and the measured ΔN_2O values fell between the two scaling law with LB overestimating and WC underestimating emissions for W >265 m. Conversely, the WC scaling law predicted well the measured average values of ΔN_2O with $v_{fden,B}$ (Figure 4b).

The impact of v_{fden} on the prediction is associated to the control that it exerts on the characteristic time of denitrification. Using $v_{fden,B}$ ($> v_{fden,M}$), obtained combing data of small headwaters streams [23] with data of larger rivers [26], the characteristic time of denitrification decreases (τ_D reduces as v_{fden} increases) and consequently denitrification, both within the benthic zone and the surface water, occurs at higher rate and therefore it results in a larger N_2O production. Accordingly, in the dimensionless framework proposed byMarzadri et al. [5], an increase of v_{fden} (i.e., a reduction of τ_D) leads to an increase in both the denitrification Damköhler numbers (Da_{DHZ} and Da_{DS}) and the associated dimensionless fluxes of N_2O ($F^*N_2O_{LB}$ and $F^*N_2O_{WC}$) that, under the same hydrological and water quality conditions,

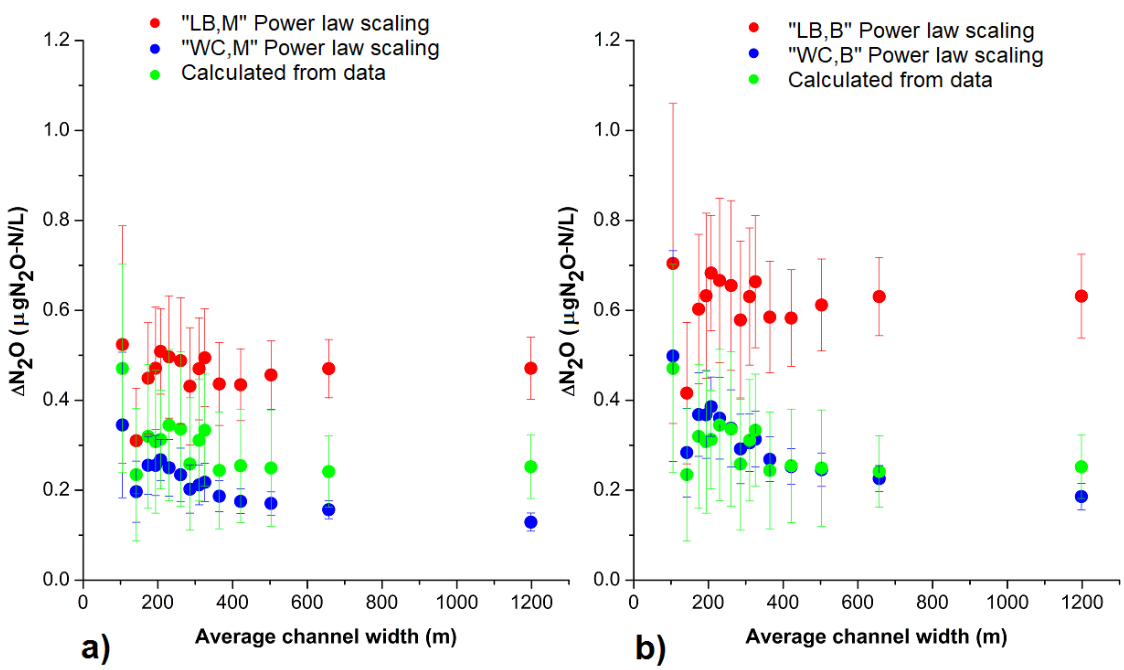

Figure 4: Comparison between predicted (red and blue bullets) and measured (green bullets) water-air nitrous oxide gradient (ΔN_2O) along the reaches of Upper Mississippi River (UMR) as a function of the average channel width. Red bullets represent predictions with the Lower Bound model (LB); while blue bullets represent predictions with the Water Column model (WC) when (a) the uptake rate of denitrification, $v_{fden,M}$, is estimated using the relation proposed by Mulholland et al. [23] and (b) $v_{fden,B}$, is estimated using the relation proposed by Böhlke et al. [26]. Data are grouped in fifteen bins (fourteen with 61 points and the last one with 62 points) and error bars represents $\pm$ standard deviation.

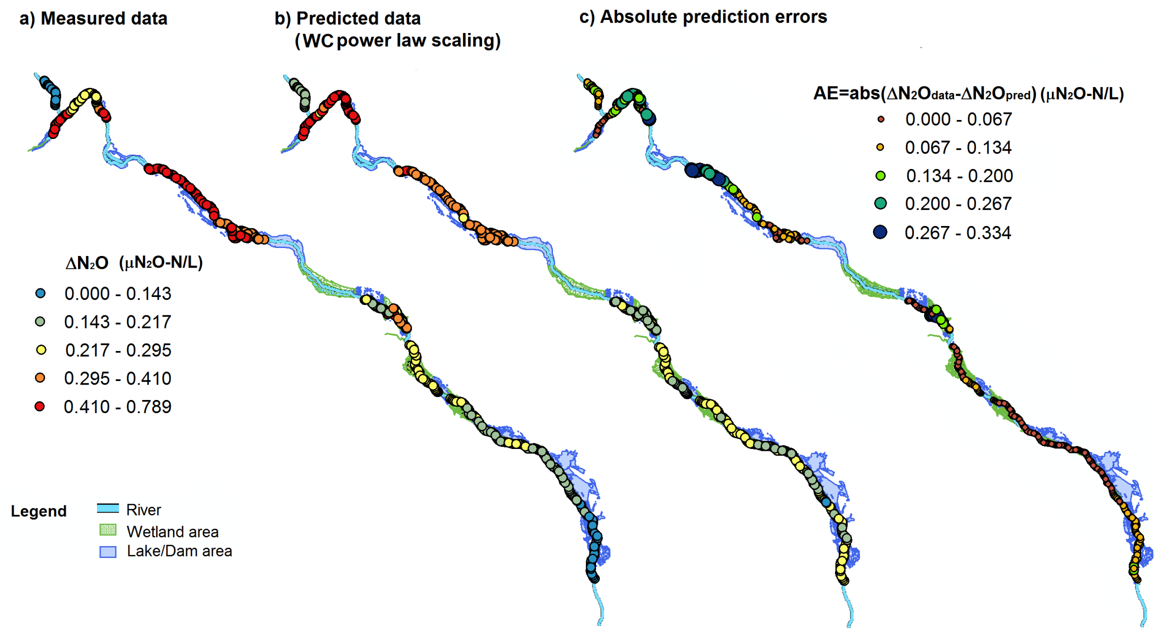

Figure 5: Pattern of variation of the water-air nitrous oxide gradient ($\Delta N_2O = [N_2O] - [N_2O]_{eq}$) along the Upper Mississippi River: (a) evaluated from measured data [13] and (b) predicted by using the WC power law scaling [5]. Subpanel (c) report the absolute error between measured and predicted ΔN_2O (AE_i).

drive LB and WC scaling laws to predict higher N_2O emissions.

Figure 4 confirms that the WC scaling law captured with satisfactory accuracy ΔN_2O measured by Turner et al. [13] along the UMR. Accordingly, Figure 5 shows the map of measured (panel a) and predicted ΔN_2O (panel b) and their absolute error (panel c) for the WC scaling law. Although with some underestimation, the WC scaling law captured the spatial distribution of ΔN_2O by matching the zone with high and low ΔN_2O. The absolute error (Figure 5c) is larger mainly in the upper part of the analyzed reach where several locks and dams are closely spaced. Within backwaters, the system may not longer behave as riverine but potentially as lentic, thereby introducing processes that the Marzadri et al.'s model [5] does not scale properly. However, the error associated with the model predictions is acceptable based on performance indexes analyzed in the present work.

These results confirms the fading importance of both hyporheic and benthic zones with size from streams to rivers. Accordingly, we conclude that the third equation for river of the Marzadri et al.'s model [5], (WC with $v_{fden} = v_{fden,B}$), was the most adequate to represent UMR data and performed well ($NSE_{WC,average} = 0.64$, $NSE_{WC,min} = 0.55$, $PBIAS_{WC,average} = -10.10\%$, $PBIAS_{min} = -15.66\%$, $RSR_{WC,average} = 0.56$, $RSR_{WC,min} = 0.27$) in predicting the water-air nitrous oxide gradient (ΔN_2O) measured by Turner et al. [13].

4. Conclusions

Results showed the robustness of Marzadri et al.'s model [5] and the importance of local measurements. The performance of the model as expected increased with better inputs and specialized information. Finally, the present work underlined how with a parsimonious predictive tool, we were able to characterize N_2O emissions along the UMR using readily available reach-scale biogeochemical measurements and hydromorphological data. The model does not require any calibration or fitting but only relays on measured or estimated quantities.

Based on these results, we suggested the use of LB scaling law with $v_{fden,M}$ for river reaches up to W =100 m and the WC scaling law with $v_{fden,B}$ for rivers reaches with W >100 m but potentially even smaller as in this study we were not able to resolve this issue (because of the limited amount of narrower reaches within this dataset, see Figure 4b). The WC scaling law may be applicable even to small widths until about W =30 m as shown in Marzadri et al. [5].

Acknowledgements

The authors thank Peter Turner for providing empirical data that supported the development of the model described in this manuscript. This publication was made possible by the NSF Idaho EPSCoR Program and by the National Science Foundation under award number IIA-1301792. AM and AB acknowledge funding from the Italian Ministry of Education, University and Research (MIUR) in the frame of the Departments of Excellence Initiative 20182022 granted to the Department of Civil, Environmental and Mechanical Engineering of the University of Trento. Any opinions, conclusions, or recommendations expressed in this material are those of the authors and do not necessarily reflect the views of the supporting agencies.

Appendix A.

Along the analyzed reach of the UMR, the average water discharge was obtained at 13 gauging stations from Fort Snelling Park(MN) to Genoa (WI) (see Figure 1) during typical summer baseflow conditions. Figure A.1 shows the trend of variation of the drainage area (DA, mi^2) and the water discharge (Q, m^3/s) as a function of the downstream distance (mi) and supports our assumptions to consider negligible the influence of the major tributaries during the sampling time (between 1^{st} and 3^{rd} of August 2015) and to expect a linear variation of Q between successive sampling points.

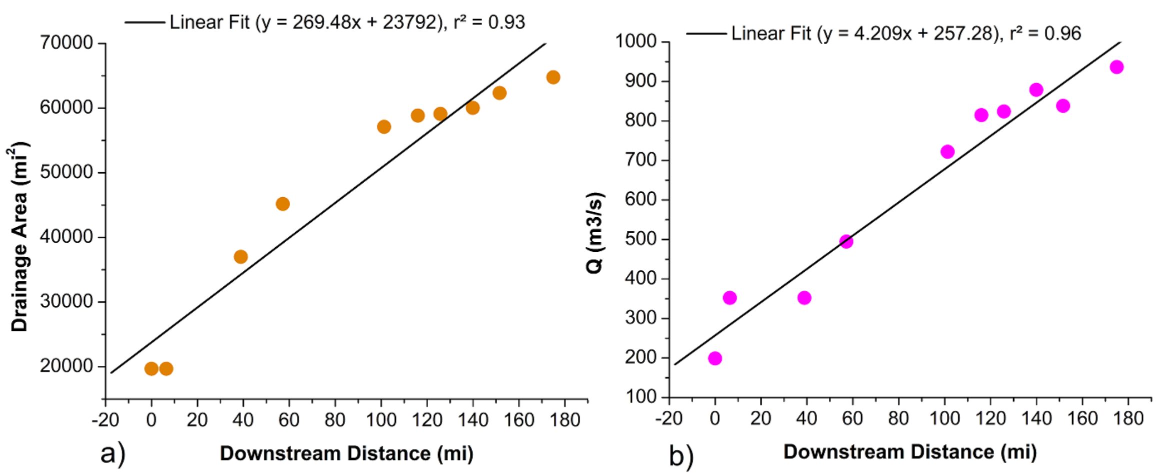

Figure A.1: Trend of variation of (a) drainage area and (b) water discharge as a function of the downstream distance from the gauging station of Lower St. Anthony Falls (MN) to the gauging station of Genoa (WI).

Starting from these assumptions and using the sufficient and necessary input parameters summarized in Table A.1 we applied the model proposed and validated by Marzadri et al. [5] to analyze which riverine environmental compartment (i. e. hyporheic zone, benthic area or water column) controls N_2O emissions.

We conclude that the WC model produces good predictions of local emissions respect to the UB and LB models as remarked by the degree of correlation between the measured ΔN_2O and the error (Absolute Error, AE_i $\mu g N_2O - N/L$) in Figure A.2. Accordingly, we expect that the total

Parameter (description)	Units	References
Latitude (cell latitude WGS84)	[Decimal Degree]	Turner et al. [13]
Longitude (cell longitude WGS84)	[Decimal Degree]	Turner et al. [13]
Q (water discharge)	[m^3/s]	USGS-USACE
s_0 (stream slope)	[$-$]	Manning's equation [33]
T (water temperature)	[°C]	Sullivan et al. [65]
d_{50} (median grain size)	[mm]	Danivory [27]
$[NO_3^-]$ (in-stream nitrate concentration)	[μmol/L]	Loken et al. [29]
$[NH_4^+]$ (in-stream ammonium concentration)	[μmol/L]	Loken et al. [29]
$[N_2O]$ (in-stream nitrous oxide concentration)	[$mgN_2O - N/L$]	Turner et al. [13]
$\%N_2O_{sat}$ (saturation percentage of nitrous oxide)	[%]	P. Turner [(a)]

[(a)] Values provided by P. Turner personal communication.

Table A.1: Sufficient and necessary input parameters to capture the N_2O emissions from the main stem of the Upper Mississippi River (UMR).

error will reduce significantly when the emissions are aggregated (integrated) over the relevant (sub)catchments.

Finally, Table A.2 and Table A.3 provide some main statistical parameters (NSE, PBIAS, RMSE and RSR) to assess the performance and the accuracy of the LB and WC model in predicting the measured ΔN_2O (mgN_2O-N/L). In particular, these tables support the results proposed in Figure 4 when v_{fden} is estimated using the relation proposed by Mulholland et al. [23] and by Böhlke et al. [26], respectively.

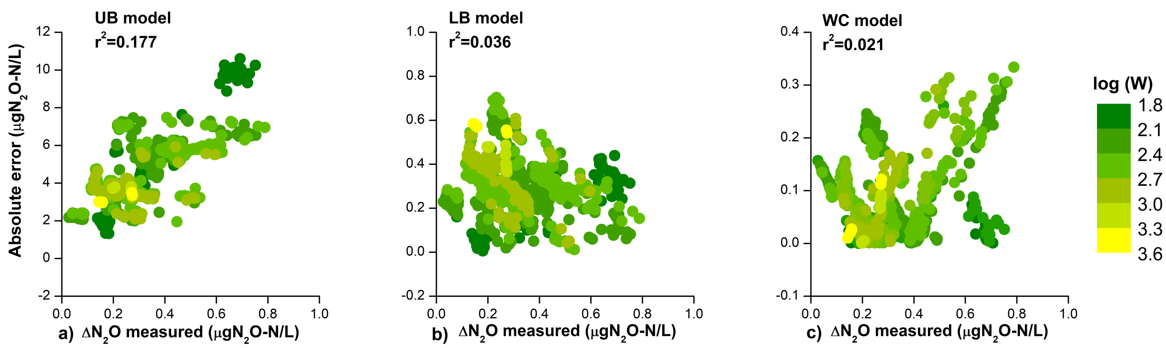

Figure A.2: Comparison between the Absolute Error (AE_i) and the measured water-air nitrous oxide gradient ($\mathrm{AE_i} = |\Delta \mathrm{N_2O_i^{obs}} - \Delta \mathrm{N_2O_i^{sim}}|$) along the Upper Mississippi River (UMR) by using: (a) the Upper Bound, UB, power law scaling; (b) the Lower Bound, LB, power law scaling and (c) the Water Column, WC, power law scaling (as in Marzadri et al. [5]). Color of the symbols shift from green to yellow as the width of the channel increases. The uptake rate of denitrification ($v_{f,denB}$) is estimated by using the equation (11) [26].

Bin	**Width**	**RMSE**		**NSE**		**PBIAS**		**RSR**	
(-)	**(m)**	$LB_{,M}$	$WC_{,M}$	$LB_{,M}$	$WC_{,M}$	$LB_{,M}$	$WC_{,M}$	$LB_{,M}$	$WC_{,M}$
1	105.08	0.087	0.151	0.856	0.570	-11.255	26.679	0.380	0.656
2	142.05	0.101	0.130	0.844	0.741	-18.192	23.162	0.394	0.509
3	173.79	0.132	0.134	0.594	0.582	-25.123	22.217	0.637	0.646
4	193.71	0.154	0.134	0.393	0.538	-31.553	21.056	0.779	0.680
5	207.14	0.169	0.129	0.148	0.506	-37.456	19.804	0.923	0.703
6	229.96	0.173	0.135	0.081	0.443	-38.588	21.137	0.959	0.746
7	260.85	0.175	0.139	0.040	0.391	-39.551	22.455	0.980	0.781
8	285.90	0.178	0.138	0.099	0.463	-42.290	22.370	0.949	0.733
9	310.34	0.178	0.138	-0.062	0.359	-43.233	23.393	1.031	0.800
10	325.49	0.177	0.139	-0.109	0.319	-43.755	24.567	1.053	0.825
11	364.24	0.180	0.137	0.010	0.426	-46.209	24.496	0.995	0.758
12	421.49	0.182	0.137	-0.103	0.377	-47.891	24.944	1.050	0.789
13	502.96	0.187	0.137	-0.175	0.364	-50.088	25.362	1.084	0.798
14	657.11	0.191	0.136	-0.266	0.362	-52.638	25.921	1.125	0.799
15	1198.10	0.195	0.136	-0.454	0.294	-54.601	27.230	1.206	0.840

Table A.2: Root Mean Square Error (RMSE), Nash Sutcliffe Efficiency Index (NSE), percentage of bias (PBIAS) and ratio of the root mean square error to the standard deviation of measured data (RSR) between measured and predicted water-air nitrous oxide gradient ($\Delta N_2O\,(\mu g N_2O - N/L)$) as a function of channel width. Data are grouped in fifteen bins (fourteen with 61 points and the last one with 62 points) with the second column representing the average channel width (m). Predictions are obtained with the Lower Bound model (LB) and the Water Column model (WC) when the uptake rate of denitrification (v_{fden}) is estimated using the relation proposed by Mulholland et al. [23] ($LB_{,M}$, $WC_{,M}$).

Bin	**Width**	**RMSE**		**NSE**		**PBIAS**		**RSR**	
(-)	**(m)**	$LB_{,B}$	$WC_{,B}$	$LB_{,B}$	$WC_{,B}$	$LB_{,B}$	$WC_{,B}$	$LB_{,B}$	$WC_{,B}$
1	105.08	0.273	0.062	-0.416	0.927	-49.616	-5.904	1.190	0.271
2	142.05	0.241	0.082	0.109	0.897	-58.820	-10.880	0.944	0.321
3	173.79	0.268	0.101	-0.663	0.763	-68.090	-12.210	1.289	0.487
4	193.71	0.292	0.110	-1.186	0.691	-76.704	-13.868	1.479	0.556
5	207.14	0.313	0.111	-1.936	0.631	-84.621	-15.664	1.713	0.607
6	229.96	0.319	0.113	-2.138	0.608	-86.130	-13.734	1.771	0.626
7	260.85	0.323	0.114	-2.267	0.595	-87.411	-11.824	1.807	0.637
8	285.90	0.325	0.113	-1.993	0.638	-91.071	-11.935	1.730	0.602
9	310.34	0.326	0.111	-2.561	0.589	-92.325	-10.451	1.887	0.641
10	325.49	0.327	0.108	-2.769	0.589	-93.018	-8.754	1.941	0.641
11	364.24	0.329	0.107	-2.298	0.651	-96.298	-8.848	1.816	0.591
12	421.49	0.330	0.107	-2.617	0.622	-98.542	-8.193	1.902	0.615
13	502.96	0.334	0.107	-2.768	0.612	-101.480	-7.584	1.941	0.623
14	657.11	0.339	0.105	-2.991	0.616	-104.890	-6.772	1.998	0.619
15	1198.10	0.344	0.104	-3.515	0.583	-107.512	-4.881	2.125	0.645

Table A.3: Root Mean Square Error (RMSE), Nash Sutcliffe Efficiency Index (NSE), percentage of bias (PBIAS) and ratio of the root mean square error to the standard deviation of measured data (RSR) between measured and predicted water-air nitrous oxide gradient ($\Delta \mathrm{N_2O}\,(\mu g N_2O - N/L)$) as a function of channel width. Data are grouped in fifteen bins (fourteen with 61 points and the last one with 62 points) with the first column representing the average channel width (m). Predictions are obtained with the Lower Bound model (LB) and the Water Column model (WC) when the uptake rate of denitrification (v_{fden}) is estimated using the relation proposed by Böhlke et al. [26] ($LB_{,B}$, $WC_{,B}$).

References

[1] J. N. Galloway, F. J. Dentener, D. G. Capone, E. W. Boyer, R. W. Howarth, S. P. Seitzinger, G. P. Asner, C. C. Cleveland, P. A. Green, E. A. Holland, D. M. Karl, A. F. Michaels, J. H. Porter, A. R. Townsend, C. J. Vöosmarty, Nitrogen Cycles: Past, Present, and Future, Biogeochemistry 70 (2004) 153–226. doi:10.1007/s10533-004-0370-0.

[2] A. Ravishankara, J. S. Daniel, R. W. Portman, Nitrous oxide (N_2O): The dominant ozone-depleting substance emitted in the 21st century, Science 326 (2009) 123–125. doi:10.1126/science.1176985.

[3] IPCC, 2014: Climate Change 2014: Synthesis Report. Contribution of Working Groups I, II and III to the Fifth Assessment Report of the Intergovernmental Panel on Climate Change [Core Writing Team, R.K. Pachauri and L.A. Meyer (eds.)], Technical Report, Geneva, Switzerland, 2014.

[4] J. J. Beaulieu, J. L. Tank, S. K. Hamilton, W. M. Wollheim, R. O. H. Jr., P. J. Mulholland, B. J. Peterson, L. R. Ashkenas, L. W. Cooper, C. N. Dahm, W. K. Dodds, N. B. Grimm, S. L. Johnson, W. H. McDowell, G. C. Poole, H. M. Valett, C. P. Arango, M. J. Bernot, A. J. Burgin, C. L. Crenshaw, A. M. Helton, L. T. Johnson, J. M. O'Brien, J. D. Potter, R. W. Sheibley, D. J. Sobota, S. M. Thomas, Nitrous oxide emission from denitrification in stream and river networks, Proc. Natl. Acad. Sci. USA 108 (2011) 214–219. doi:10.1073/pnas.1011464108.

[5] A. Marzadri, M. M. Dee, D. Tonina, A. Bellin, J. L. Tank, Role of surface and subsurface processes in scaling N_2O emissions along riverine networks, PNAS Proceeding of the National Academy of Sciences of the United States of America 114 (2017) 4330–4335. doi:10.1073/pnas.1617454114.

[6] S. P. Seitzinger, C. Kroeze, Global distribution of nitrous oxide production and n inputs in freshwater and coastal marine ecosystems, Global Biogeochemical Cycles 12 (1988) 93–113. doi:10.1029/97GB03657.

[7] J. J. Cole, N. F. Caraco, Emissions of nitrous oxide (n2o) from a tidal, freshwater river, the hudson river, new york, Environmental Science Technology 35 (2001) 991–996. doi:10.1021/es0015848.

[8] A. Syakila, C. Kroeze, The global nitrous oxide budget revisited, Greenhouse Gas Measurement and Management 1 (2012) 17–26. doi:10.3763/ghgmm.2010.0007.

[9] A. M. Quick, W. J. Reeder, T. B.Farrell, D. Tonina, K. P.Feris, S. G. Benner, Nitrous oxide from streams and rivers: A review of primary biogeochemical pathways and environmental variables, Earth-Science Rev. 191 (2019) 224–262. doi:10.1016/j.earscirev.2019.02.021.

[10] H. Baulch, S. Schiff, R. Maranger, P.J.Dillon, Nitrogen enrichment and the emission of nitrous oxide from streams, Global Biogeochem. Cycles 25 (2011) GB4013. doi:10.1029/2011GB004047.

[11] M. S. Rosamond, S. J. Thuss, S. L. Schiff, Dependence on riverine nitrous oxide emissions on dissolved oxygen levels, Nat. Geosci. 5 (2012) 715–718. doi:10.1038/ngeo1556.

[12] A. V. Borges, F. Darchambeau, C. R. Teodoru, T. R. Marwick, F. Tamooh, N. Geeraert, F. O. Omengo, F. Guérin, T. Lambert, C. Morana, E. Okuku, S. Bouillon, Globally significant greenhouse-gas emissions from African inland waters, Nature Geosci. 8 (2015) 637–642. doi:10.1038/NGEO2486.

[13] P. A. Turner, T. J. Griffis, J. M. Baker, X. Lee, J. T. Crawford, L. C. Loken, R. T. Venterea, Regional-scale controls on dissolved nitrous oxide in the Upper Mississippi River, Geophys. Res. Lett. 43 (2016) 4400–4407. doi:10.1073/pnas.1503.

[14] M. Hu, D. C. abd R.A. Dahlgren, Mmodeling nitrous oxide emission from rivers: a global assessmen, Glob. Chang. Biol. 22 (2015) 3566–3582. doi:10.1111/gcb.13351.

[15] A. Marzadri, D. Tonina, A. Bellin, J. L. Tank, A hydrologic model demonstrates nitrous oxide emissions depend on streambed morphology, Geophys. Res. Lett. 41 (2014) 5484–5491. doi:10.1002/2014GL060732.

[16] C. R. Teodoru, F. C. Nyoni, A. V. Borges, F. Darchambeau, I. Nyambe, S. Bouillon, Spatial variability and temporal dynamics of greenhouse gas (CO_2, CH_4, N_2O) concentrations and uxes along the Zambezi River mainstem and major tributaries, Biogeosci. 12 (2014) 2431–2453. doi:10.5194/bg-12-2431-2015.

[17] H. Lin, M. Dai, S.-J. Kao, L. Wang, E. Roberts, J.-Y. T. Yang, T. H. T., B. He, Spatiotemporal variability of nitrous oxide in a large eutrophic estuarine system: The Pearl River Estuary, China, Mar. Chem. 182 (2016) 14–24. doi:10.1016/j.marchem.2016.03.005.

[18] J. J. Beaulieu, C. P. Arango, J. L. Tank, The effects of season and agriculture on nitrous oxide production in headwater streams, Journal of Environmental Quality 38 (2009) 637–646. doi:10.2134/jeq2008.0003.

[19] S. Hinshaw, R. Dahlgren, Dissolved nitrous oxide concentrations and fluxes from the eutrophic San Joaquin River, California, Environ. Sci. Technol. 47 (2013) 1313–1322. doi:10.1021/es301373h.

[20] J. Harrison, P. Marson, Patterns and controls of nitrous oxide emissions from waters draining a subtropical agricultural valley, Glob. Biogeochem. Cycl. 17 (2003) 1080. doi:10.1029/2002GB001991.

[21] J. Venkiteswaran, M. S. Rosamond, S. L. Schiff, Nonlinear response of riverine N_2O uxes to oxygen and temperature, Environ. Sci. Technol. 48 (2014) 1566–1573. doi:10.1021/es500069j.

[22] J. Garnier, G. Billen, G. Vilain, A. Martinez, M. Silvestre, E. Mounier, F. Toche, Nitrous oxide (N_2O) in the Seine river and basin: observations and budgets, Agr. Ecosyst. Environ. 133 (2009) 123–233. doi:10.1016/j.agee.2009.04.024.

[23] P. J. Mulholland, A. M. Helton, G. C. Poole, R. O. H. Jr, S. K. Hamilton, B. J. Peterson, J. L. Tank, L. R. Ashkenas, L. W. Cooper, C. N. Dahm, W. K. Dodds, S. E. G. Findlay, S. V. Gregory, N. B. Grimm, S. L. Johnson, W. H. McDowell, J. L. Meyer, H. M. Valett, J. R. Webster, C. P. Arango, J. J. Beaulieu, M. J. Bernot, A. J. Burgin, C. L. Crenshaw, L. T. Johnson, B. R. Niederlehner, J. M. O'Brien, J. D. Potter, R. W. Sheibley, D. J. Sobota, S. M. Thomas, Stream denitrification across biomes and its response to anthropogenic nitrate loading, Nature 452 (2008) 202–206. doi:10.1038/nature06686.

[24] J. J. Beaulieu, C. P. Arango, S. K. Hamilton, J. L. Tank, The production and emission of nitrous oxide from headwater in the Midwestern United States, Global Change Biology 14 (2008) 878–894. doi:10.1111/j.1365-2486.2007.01485.x.

[25] C. J. Ocampo, C. E. Oldham, M. Sivapalan, Nitrate attenuation in agricultural catchments: Shifting balances between transport and reaction, Water Resour. Res. 42 (2006) W01408. doi:10.1029/2004WR003773.

[26] J. K. Böhlke, R. C. Antweiler, J. W. Harvey, A. E. Laursen, L. K. Smith, R. L. Smith, M. A. Voytek, Multi-scale measurements and modeling of denitrification in streams with varying flow and nitrate concentration in the Upper Mississippi River basin, USA, Biogeochem. 93 (2009) 117–141. doi:10.1007/s10533-008-9282-8.

[27] Sedimentation in the Upper Mississippi River Basin, Technical Report, St. Louis, Missouri (USA), 2006.

[28] J. W. F. Remo, R. A. Heine, B. S. Ickes, Particle size distribution of main-channel-bed sediments along the upper Mississippi River, USA, Geomorphology 264 (2016) 118–131. doi:10.1016/j.geomorph.2016.04.012.

[29] L. C. Loken, J. T. Crawford, M. M. Dornblaser, J. Houser, P. A. Turner, R. G. Striegl, E. H. Stanley, Limited nitrate retention in the Upper Mississippi River, Environmental Research Letters 13 (2018). doi:10.1088/1748-9326/aacd51.

[30] J. T. Crawford, L. C. Loken, N. J. Casson, C. Smith, A. G. Stone, L. A. Winslow, High-speed limnology: Using advanced sensors to investigate spatial variability in biogeochemistry and hydrology, Environ. Sci. Technol. 49 (2015) 442–450. doi:10.1021/es504773x.

[31] Upper Mississippi River Pool 8 Long Term Resource Monitoring - 2015 Status Report, Technical Report, Mississippi River Monitoring Field Station, La Crosse, Wisconsin (USA), 2016.

[32] Z. F. Miller, T. M. Pavelsky, G. H. Allen, Quantifying river form variations in the mississippi basin using remotely sensed imagery, Hydrol. Earth Syst. Sci 18 (2014) 4883–4895. doi:10.5194/hess-18-4883-2014.

[33] C. W. Fetter, Applied Hydrogeology, 4 ed., Prentice Hall, Upper Saddle River, N.J., 2001.

[34] Mississippi River (Pool 2) 2-D ADH Model Development Final Report, Technical Report, St. Louis, Missouri (USA), 2001.

[35] D. R. Montgomery, J. M. Buffington, Channel-reach morphology in mountain drainage basins, GSA Bulletin 109 (1997) 596–611.

[36] M. S. Yalin, Geometrical properties of sand waves, J. Hydraul. Div-ASCE 90 (1964) 105–119.

[37] H. V. Shen, H. M. Fehlman, C. Mendoza, Bed form resistances in open channel flows, J. Hydraul. Eng-ASCE 116 (1990) 799–815.

[38] J. D. Gomez-Velez, J. W. Harvey, M. B. Cardenas, B. Kiel, Denitrification in the Mississippi River network controlled by flow through river bedforms, Nat. Geosci. 8 (2015) 941–945. doi:10.1038/ngeo2567.

[39] P. A. Domenico, F. W. Schwartz, Physical and chemical hdrogeology, 6 ed., Wiley, New York, United States, 1990.

[40] D. Tonina, F. P. J. de Barros, A. Marzadri, A. Bellin, Does streambed heterogeneity matter for hyporheic residence time distribution in sand-bedded streams?, Advances in Water Resources 96 (2016) 120–126. doi:10.1016/j.advwatres.2016.07.009.

[41] P. J. Mulholland, H. M. Valett, J. R. Webster, S. A. Thomas, L. W. Cooper, S. K. Hamilton, B. J. Peterson, Stream denitrification and total nitrate uptake rates measured using a field ^{15}N tracer addition approach, Limnol. Oceanogr. 49 (2004) 809–820. doi:10.4319/lo.2004.49.3.0809.

[42] FPC, Channel Assessment Procedure Field Guidebook, in: Forest Practice Code, British Columbia Ministry of Forest, Vancouver, BC., 1996, pp. 1–95.

[43] J. M. Buffington, D. R. Montgomery, Geomorphic classification of rivers, in: J. Shroder, E. Whol (Eds.), Treatise on Geomorphology, Academic Press., San Diego, 2013, pp. 730–767.

[44] A. H. Elliott, N. H. Brooks, Transfer of nonsorbing solutes to a streambed with bedforms: Theory, Water Resour Res 33 (1997a) 123–136. doi:10.1029/96WR02783.

[45] J. C. Rutherford, River Mixing, John Wiley and Sons, Chichester, England, 1994.

[46] B. Jähne, K. O. Münnich, R. Bösinger, A. Dutzi, W. Huber, P. Libner, On the parameters influencing air-water gas exchange, J. Geophys Res-Oceans 92 (1987) 1937–1949. doi:10.1029/JC092iC02p01937.

[47] R. Wanninkhof, Relation between wind speed and gas exchange over the ocean, J. Geophys. Res. 97 (1992) 7373–7382. doi:10.1029/92JC00188.

[48] P. A. Raymond, C. J. Zappa, D. Butman, T. L. Bott, J. Potter, P. J. Mulholland, A. E. Laursen, W. H. McDowell, D. Newbold, Scaling the gas transfer velocity and hydraulic geometry in streams and small rivers, Limnology and Oceanography: Fluids and Environments 2 (2012) 41–53. doi:10.1215/21573689-1597669.

[49] J. E. Nash, J. V. Sutcliffe, River flow forecasting through conceptual models part I - A discussion of principles, J. Hydrol. 10 (1970) 282–290. doi:10.1016/0022-1694(70)90255-6.

[50] D. N. Moriasi, J. Arnold, M. V. Liew, R. Bingner, R. Harmel, , T. Veith, Model evaluation guidelines for systematic quantification of accuracy in watershed simulations, Transactions of the ASABE 50 (2007) 885–900. doi:10.13031/2013.23153.

[51] T. Liu, X. Xia, S. Liu, X. Mou, Y. Qiu, Acceleration of denitrification in turbid rivers due to denitrification occurring on suspended sediment in oxic waters, Environ. Sci. Technol. 47 (2013) 4053–4061. doi:10.1021/es304504m.

[52] A. J. Reisinger, J. L. Tank, E. J. Rosi-Marshall, R. O. H. Jr., M. A. Baker, The varying role of water column nutrient uptake along river continua in contrasting landscapes, Biogeochemistry 125 (2015) 115–131. doi:10.1007/s10533-015-0118-z.

[53] J. T. Crawford, L. C. Loken, E. G. S. E. H. Stanley, M. M. Dornblaser, R. G. Striegl, Basin scale controls on CO2 and CH4 emissions from the Upper Mississippi River, Geophys. Res. Lett. 43 (2016) 1973–1979. doi:10.1002/2015GL067599.

[54] L. B. Leopold, T. Maddock, The hydraulic geometry of stream channels and some physiographic implications, U.S. Government Printing Office 57 (1953).

[55] N. E. M. Asselman, Fitting and interpretation of sediment rating curves, J. of Hydrol. 234 (2000) 228–248. doi:10.1016/S0022-1694(00)00253-5.

[56] J. A. Warrick, Trend analyses with river sediment rating curves, Hydrol. Process. 29 (2015) 936–949. doi:10.1002/hyp.10198.

[57] W. J. Reeder, A. M. Quick, T. B. Farrell, S. G. Benner, K. P. Feris, A. Marzadri, D. Tonina, A flowline-scale, predictive model of nitrous oxide emissions from the hyporheic zone of streams, Water Resour. Res. under review (2018).

[58] J. W. Harvey, J. K. Böhlke, M. A. Voytek, D. Scott, C. R. Tobias, Hyporheic zone denitrification: Controls on effective reaction depth and contribution to whole-stream mass balance, Water Resour. Res. 49 (2013) 6298–6316. doi:10.1002/wrcr.20492.

[59] R. B. Alexander, R. A. Smith, G. E. Schwarz, Effect of stream channel size on the delivery of nitrogen to the Gulf of Mexico, Nature 403 (2000) 758–761. doi:10.1038/35001562.

[60] B. Peterson, W. M. Wollheim, P. J. Mulholland, J. R. Webster, J. L. Meyer, J. L. Tank, E. Martí, W. B. Bowden, H. M. Valett, A. E. Hershey, W. H. McDowell, W. K. Dodds, S. K. Hamilton, S. Gregory, D. D. Morrall, Control of nitrogen export from watershed by headwater streams, Nature 292 (2001) 86–89. doi:10.1126/science.1056874.

[61] S. P. Seitzinger, R. V. Styles, E. W. Boyer, R. B. Alexander, G. Billen, R. W. Howarth, B. Mayer, N. van Breemen, Nitrogen retention in rivers: model development and application to watersheds in the northeastern U.S.A., Biogeochemistry 57 (2002) 199–237. doi:10.1023/A:1015745629794.

[62] M. J. Bernot, W. K. Dodds, Nitrogen retention, removal, and saturation in lotic ecosystems, Ecosystems 8 (2005) 442–453. doi:10.1007/s10021-003-0143-y.

[63] W. M. Wollheim, C. J. Vörösmarty, B. J. Peterson, S. P. Seitzinger, C. S. Hopkinson, Relationship between river size and nutrient removal, Geophys. Res. Lett. 33 (2006) L06410. doi:10.1029/2006GL025845.

[64] W. M. Wollheim, B. J. Peterson, L. A. Deegan, J. E. Hobbie, B. Hooker, W. B. Bowden, K. J. Edwardson, D. B. Arscott, A. E. Hershey, J. Finlay, Influence of stream size on ammonium and suspended particulate nitrogen processing, Limnology and Oceanography 46 (2001) 1–13. doi:10.4319/lo.2001.46.1.0001.

[65] J. Sullivan, S. Manoyan, R. Zdanowicz, Upper Mississippi River Water Quality Assessment Report, Sponsored by Upper Mississippi River Conservation Committee Water Quality Technical Section (2002) 1–199.